View metadata, citation and similar papers at core.ac.uk
brought to you by CORE
provided by NASA Technical Reports Server

Effect of EMIC Wave Normal Angle Distribution on Relativistic Electron Scattering in Outer RB

G. V. Khazanov

NASA, Marshall Space Flight Center, Huntsville, Alabama, USA

K. V. Gamayunov

NASA, Marshall Space Flight Center, Huntsville, Alabama, USA

Short title: RB ELECTRON SCATTERING BY EMIC WAVES

Abstract. We present the equatorial and bounce–average pitch–angle diffusion coefficients for scattering of relativistic electrons by the H^+–mode of EMIC waves. Both the model (prescribed) and self–consistent distributions over the wave normal angle are considered. The main results of our calculation can be summarized as follows: First, in comparison with field–aligned waves, the intermediate and highly oblique waves reduce the pitch–angle range subject to diffusion, and strongly suppress the scattering rate for low energy electrons ($E < 2$ MeV). Second, for electron energies greater than ~ 5 MeV, the $|n| = 1$ resonances operate only in a narrow region at large pitch-angles, and despite their greatest contribution in case of field–aligned waves, cannot cause electron diffusion into the loss cone. For those energies, oblique waves at $|n| > 1$ resonances are more effective, extending the range of pitch–angle diffusion down to the loss cone boundary, and increasing diffusion at small pitch–angles by orders of magnitude.

1. Introduction

The flux of outer–zone relativistic electrons (above 1 MeV) is extremely variable during geomagnetic storms. The competition between loss and acceleration, both of which are enhanced during storm periods, determines the resulting relativistic electron flux level in the Earth's outer radiation belt (RB) [e. g., *Summers et al.,* 2004; *Reeves et al.,* 2003; *Green et al.,* 2004]. During the main phase, the relativistic electron flux may decrease by up to two or three orders of magnitude. Analyzing 256 geomagnetic storms during the period 1989–2000, *Reeves et al.* [2003] found that 53 % of the storms lead to higher flux levels during the storm recovery phase in comparison to pre–storm levels, 28 % produce no change, and 19 % lead to net decrease in flux levels. The large electron flux decrease during the main storm phase is usually associated with either the *Dst* effect, when the relativistic electrons adiabatically respond to the inflation of the magnetic field lines caused by the formation of a partial ring current (RC) [*Kim and Chan,* 1997], and/or the drift out the magnetopause boundary [*Li et al.,* 1997], and/or the nonadiabatic scattering into the loss cone due to cyclotron interaction with electromagnetic ion cyclotron (EMIC) waves [*Thorne and Kennel,* 1971; *Lyons and Thorne,* 1972; *Summers and Thorne,* 2003; *Albert,* 2003; *Thorne et al.,* 2005].

Precipitation of the outer RB electrons due to resonant pitch–angle scattering by EMIC waves is considered to be one of the more important loss mechanisms, so in the present study we concentrate on this process only. This mechanism was suggested in early theoretical studies three and half decades ago [*Thorne and Kennel,* 1971; *Lyons*

and Thorne, 1972], however, direct experimental evidence of EMIC wave–induced relativistic electron precipitation is scanty because of a lack of concurrent measurements of low altitude precipitating electrons and magnetically conjugate equatorial waves. Recently, data from balloon–borne X–ray instruments provided indirect but strong evidence for EMIC wave–induced loss of outer–zone relativistic electrons in the late afternoon–dusk MLT sector [*Foat et al.,* 1998; *Lorentzen et al.,* 2000; *Millan et al.,* 2002]. These observations stimulated theoretical and statistical studies which demonstrated that this mechanism for MeV electron pitch–angle diffusion can operate at the strong diffusion limit, and can compete with relativistic electron depletion caused by the *Dst* effect during the initial and main phases of a storm [*Summers and Thorne,* 2003; *Albert,* 2003; *Loto'aniu et al.,* 2006; *Meredith et al.,* 2003].

Although the effectiveness of relativistic electron scattering by EMIC waves depends strongly on the wave spectral properties, unrealistic assumptions regarding the wave angular spread were made in previous theoretical studies. That is, only field–aligned or quasi field–aligned EMIC waves were considered as a driver for relativistic electron precipitation (except *Glauert and Horne* [2005] where a calculation for prescribed oblique wave distributions was presented for the H^+–mode). At the same time, there is growing experimental [*Anderson et al.,* 1996; *Denton et al.,* 1996] and theoretical [*Khazanov et al.,* 2006a; 2006b] evidence that EMIC waves can be highly oblique; EMIC waves occur not only in the source region, i.e. at small wave normal angles, but also in the entire region, even near 90 degrees. This can dramatically change the effectiveness of relativistic electron scattering by EMIC waves. In the present study, we calculate the

pitch–angle diffusion coefficients using the wave normal distributions provided by our self–consistent RC–EMIC wave model [*Khazanov et al.,* 2006a], and quantify the effect of oblique EMIC waves on outer RB relativistic electron scattering.

This article is organized as follows: In Section 2 we outline some outstanding data analysis issues which, in our opinion, should be addressed in order to extract the correct polarization properties of EMIC waves from observations. In Section 3, using model wave spectra and prescribed plasma parameters, we consider the effect of oblique EMIC waves on relativistic electron scattering. In Section 4, we present the bounce–averaged diffusion coefficients based on the wave spectra from a self–consistent RC–EMIC wave model. Finally, in Section 5 we summarize.

2. Field–Aligned and Oblique EMIC Waves: Observations and Theory

In order to estimate the wave normal angle, the minimum variance direction is found from the wave observations. For a plane EMIC wave, the magnetic fluctuation, $\delta\mathbf{B}$, and wave vector $\mathbf{k}$ are related by $\mathbf{k} \cdot \delta\mathbf{B} = 0$. So the fluctuation $\delta\mathbf{B}$ is entirely in the plane perpendicular to $\mathbf{k}$, and the minimum variance direction $\mathbf{e_{min}}$ is parallel to $\mathbf{k}$. In this case, the angle between $\mathbf{e_{min}}$ and external magnetic field ($\mathbf{B_0}$), θ_{min}, gives the angle between $\mathbf{k}$ and $\mathbf{B_0}$, θ_{kB_0}. *Fraser* [1985] and *Ishida et al.* [1987] found that θ_{min} was generally less than 30°, and for most waves $\theta_{min} < 15°$. Then, assuming that the observed waves could be represented by a single plane mode, they related the derived

angle to the wave normal angle as $\theta_{kB_0} = \theta_{min}$.

Another important spectral wave characteristic is ellipticity, ϵ, which is closely related to θ_{kB_0}. For a plane EMIC wave, ϵ determines θ_{kB_0}, and vice versa, if the plasma properties and wave frequency are specified. The ellipticity is defined as the ratio of the minor to the major axis of the wave polarization ellipse in the plane perpendicular to $\mathbf{B_0}$ with $\epsilon = -1$ for left circular, $\epsilon = 0$ for linear, and $\epsilon = +1$ for right circular polarization. The EMIC waves observed near the equator are mainly linear or left–hand polarized with some admixture of the right–hand polarization [*Anderson et al.,* 1992; *Fraser and Nguyen,* 2001; *Meredith et al.,* 2003; *Ishida et al.,* 1987]. There is a clear tendency for the polarization to become more linear with increasing magnetic latitude. The observation of a significant number of linear polarized events occurring near the equator cannot be explained by the polarization reversal from left–handed through linear to right–handed at the crossover frequency, as suggested by *Young et al.* [1981], and is intriguing because of small θ_{min} [*Meredith et al.,* 2003]; waves should be highly oblique for $\epsilon \approx 0$, which is inconsistent with the reported θ_{kB_0} (actually θ_{min}) and ϵ.

Let us now outline the two outstanding data analysis problems which, in our opinion, are closely related to the above inconsistency, and should be resolved first in order to extract the correct wave polarization properties from the observations. Fast Fourier Transform (FFT) analysis has become the conventional method for quantitative determination of the wave polarization and minimum variance direction [*Means,* 1972; *Arthur et al.,* 1976]. Fourier analysis implicitly assumes that the analyzed signal is a superposition of components with different frequencies and that during the analyzed

time segment each component has no random phase variations (stationary signal) in both time and orientation (for vector signal) [*Anderson et al.,* 1996]. For example, FFT analysis applied to a series of wave packets with the same frequency but with arbitrary relative phases will produce a "broad" range of frequencies. *Anderson et al.* [1996] showed that when the magnetic fluctuations are not stationary in time and, specifically, when the axes of the wave polarization ellipse fluctuate in azimuth, then the FFT analysis of the minimum variance direction and polarization are unreliable. The reason is that the time window for analysis contains numerous randomly fluctuating wave packets. The time window, in turn, is determined by the desired frequency resolution, which is the reciprocal of the window length.To achieve acceptable frequency resolution, time segments of several minutes or even much longer are typically used [*Fraser,* 1985; *Ishida et al.,* 1987].

Analyzing 46 EMIC events, each 30 to 60 minutes long, from 44 different days, *Anderson et al.* [1996] found that polarization parameters vary over a time period of a few wave periods. This allows them to conclude that significant polarization axis fluctuations are a common feature of EMIC waves and hence that nonstationarity effects are a general property of waves in magnetosphere. The stationarity timescales are too short for standard FFT analysis, and to address this problem *Anderson et al.* [1996] developed a minimum variance technique which operates on timescales of a few wave periods. They called this technique a "wave step", and showed how to determine which method, FFT and/or wave step, is best for a given data set. Note that despite using very short time windows, the wave step procedure achieves good frequency precision

[*Anderson et al.,* 1996]. Compared to the wave packet technique, the decomposition of a nonstationary signal using the traditional FFT analysis can yield a dramatic underestimate of the minimum variance polar angle (often more than 45°) and an overestimate of $|\epsilon|$. The maximum disagreement occurs for linear polarization. This is a significant problem because the minimum variance direction determines the EMIC wave normal vector orientation which is crucial for resolving major outstanding questions of the EMIC wave generation, propagation, and damping. Using the more reliable wave step polarization results, *Anderson et al.* [1996] presented the first analysis of nearly linear polarized waves for which the polarization properties have been determined. They found a significant number of wave intervals with $\theta_{min} > 70°$, the highest θ_{min} ever reported.

However, it should be noted that $\theta_{min} \neq \theta_{kB_0}$ if $\delta\mathbf{B}$ is due to a superposition of plane waves with different azimuthal angles [*Anderson et al.,* 1996; *Hoppe et al.,* 1982]. A quantitative analysis of the effects of superposition on the observed wave polarization properties has been presented by *Denton et al.* [1996]. Using data from the AMPTE/CCE spacecraft, *Denton et al.* [1996] made a detailed comparison between the observed polarization properties of EMIC waves and those predicted by theory, where the theoretical linear wave properties were based on the plasma parameters observed during EMIC events, calculated using the linear dispersion code XWHAMP [*Schwarz and Denton,* 1991]. *Denton et al.* [1996] analyzed the ellipticity, the ratio of parallel (along B_0) magnetic fluctuation δB_z to the major axis component of the elliptical perturbation in the perpendicular plane δB_{major}, and the phase angle $\phi_{z-major}$ between

δB_z and δB_{major}. They found that the observed polarization properties are inconsistent with the assumption that the resultant observed waves are from a single plane wave. Namely, (1) the observed ellipticity (ϵ^{obs}) data plotted versus θ_{min} are at great variance to the theoretical curves, (2) while $\delta B_z/\delta B_{major} = \epsilon^{obs} \tan\theta_{min}$ if the single wave assumption is valid, the observed distribution of $\delta B_z/\delta B_{major}$ appears to be relatively independent of $\epsilon^{obs} \tan\theta_{min}$, and (3) the distribution of $\phi_{z-major}$, while peaked around 90° (that is consistent with the single wave assumption for guided mode), is often quite broad. In order to explain the discrepancies, *Denton et al.* [1996] developed a simple model with two constituent waves in various azimutal orientations and temporal phase relations. They showed that the distribution of observed polarization properties can be well accounted for as resulting from a superposition of more than one plane wave, and furthermore, the required constituent waves have properties consistent with linear dispersion theory. When there is a superposition of waves, the instantaneously observed polarization characteristics do not reliably reflect the constituent wave properties and the minimum variance direction cannot be associated with wave vector. *Denton et al.* [1996] therefore concluded that wave polarization analysis, which assumes that the observed fluctuations are due to the single plane wave, is not valid. Particularly, they noted that determination of wave vector orientation by means of minimum variance analysis is especially susceptible to error, since even the median value of θ_{min} gives an unreliable estimate to θ_{kB_0}.

The effects of wave superposition on the observed polarization characteristics are generally as large or larger than the variations between parameters associated with

linear wave dispersion. Nevertheless, although individual resultant wave properties can be quite different from those of the constituent waves, the entire distribution from an ensemble of resultant waves has some properties in common with the constituent waves. Assuming that both constituent waves have the same ellipticity, ϵ^C, and wave normal angle, $\tan\theta^C_{kB_0}$, *Denton et al.* [1996] showed that the median value of the resultant ellipticity $\overline{\epsilon^R}$ is equal to the constituent ellipticity ϵ^C. Similarly, they showed that the median value $\overline{\delta B^R_z/\delta B^R_{major}}$ is close to $\overline{\epsilon^R}\tan\theta^C_{kB_0}$. In this way they inferred the essential polarization properties of constituent waves from the observations. For example, for the 1985–018 EMIC wave event, they found $\epsilon^C = 0.07$ and $\theta_{kB_0} = 77^\circ$ that is consistent with theoretical wave linear properties based on the plasma parameters observed during the event.

In general, the observed EMIC waves have more than two constituent waves. So even if the correct FFT and/or wave step method is used, there still exists an uncertainty which has to be resolved in order to extract the correct polarization properties from observations. (We should emphasize that the simple model of *Denton et al.* [1996] has been remarkably successful at qualitatively explaining the distribution of the observed polarization parameters.) So combinations of reliable data and theoretical models should be utilized in order to obtain the power spectral density of EMIC waves over the entire outer RB throughout the different storm phases.

Recently *Khazanov et al.* [2006a] presented the global self–consistent theoretical model of interacting RC and EMIC waves. This model explicitly includes the wave generation and damping, propagation, refraction, reflection and tunneling in a multi–ion

magnetospheric plasma. To the best of our knowledge, this is the only model which self–consistently obtains the spatial (3D), temporal and spectral characteristics of EMIC waves on global magnetospheric scales during the different storm phases. This model predicts that the equatorial wave normal angle distribution for He^+–mode EMIC waves can occupy not only the source region, i. e. the region of small wave normal angles, but all wave normal angles, including those near 90°. Although this contradicts to the results of *Fraser* [1985] and *Ishida et al.* [1987], it is in qualitative agreement with the results of the data analysis by *Anderson et al.* [1996] and *Denton et al.* [1996] which were obtained with a more reliable technique.

3. Equatorial Pitch–Angle Diffusion Coefficient: Model Calculations

To consider the effect of the wave normal angle distribution on the effectiveness of relativistic electron scattering by EMIC waves, we first calculate the local pitch–angle diffusion coefficient. The discussion and results related to the bounce and drift average diffusion coefficients can be found, for example, in [*Albert,* 2003; *Summers and Thorne,* 2003; *Loto'aniu et al.,* 2006]. In the present study, we use the relativistic form of the diffusion coefficient from our previous papers [e. .g, *Khazanov et al.,* 2003]. The recent extensive statistical analysis of EMIC events by *Meredith et al.* [2003] showed that in about 11 % of the observations, the minimum electron resonant energy fell below 2 MeV, and that most of these cases were associated with wave frequencies just below

the helium gyrofrequency. So in what follows we take into account only the He^+–mode of EMIC waves. Although the model by *Khazanov et al.* [2006a] provides self–consistent spectra for the He^+–mode, in order to eliminate an unnecessary complication the analysis in this Section is done for prescribed wave spectra and plasma parameters. First, a Gaussian frequency spectrum,

$$B^2(\omega) \sim \exp\left\{-\frac{(\omega-\omega_m)^2}{\delta\omega^2}\right\}, \quad \omega_{LC} \le \omega \le \omega_{UC}, \tag{1}$$

is assumed, where following *Summers and Thorne* [2003] and/or *Albert* [2003], $\omega_{LC} = \omega_m - \delta\omega$, $\omega_{UC} = \omega_m + \delta\omega$, $\omega_m = 3\Omega_{O^+}$, and $\delta\omega = 0.5\Omega_{O^+}$, where Ω_{O^+} is the gyrofrequency of O^+. Second, the wave normal angle distribution is assumed to be a constant inside a specified region and zero otherwise. Below we consider the following three cases,

$$\begin{aligned} &\text{Case A}: \quad 0^\circ \le \theta < 30^\circ,\ 150^\circ < \theta \le 180^\circ, \\ &\text{Case B}: \quad 30^\circ \le \theta < 60^\circ,\ 120^\circ < \theta \le 150^\circ, \\ &\text{Case C}: \quad 60^\circ \le \theta \le 89^\circ,\ 91^\circ \le \theta \le 120^\circ, \end{aligned} \tag{2}$$

which allow us to model field–aligned, intermediate and highly oblique wave spectra. Note that the diffusion coefficient is a linear functional of the wave spectral intensity, and the sum of cases A, B, and C describe a situation when EMIC wave energy is evenly distributed in the entire wave normal angle region, $0^\circ \le \theta \le 180^\circ$ (we excluded the region near 90° because of the Landau damping by thermal electrons [e. g., *Thorne and Horne,* 1992; *Khazanov et al.,* 2006b]). For benchmark purposes we also calculate the

diffusion coefficients for a Gaussian distribution over $x = \tan\theta$ ($0° \leq \theta \leq 15°$) which has been used by *Albert* [2003]. In each case, the wave amplitude is normalized to ensure

$$\int_{\omega_{LC}}^{\omega_{UC}} \mathrm{d}\omega \int_0^{\pi} \mathrm{d}\theta B^2(\omega,\theta) = 1 \text{ nT}^2. \tag{3}$$

Finally, to specify the ion content we follow *Summers and Thorne* [2003], *Albert* [2003], *Meredith et al.* [2003], *Loto'aniu et al.* [2006], and just prescribe the storm time ion composition to be 70% H^+, 20% He^+, and 10% O^+.

Results of our calculation are presented in Figure 1. The first row shows the local (equatorial) pitch–angle diffusion coefficients, and the second row shows the corresponding resonant numbers averaged with the following weights: Figure 1

$$\left\langle n(E,\alpha) \right\rangle = \frac{\sum_n n \int_{\omega_{LC}}^{\omega_{UC}} \mathrm{d}\omega \int_0^{\pi} \mathrm{d}\theta D^n_{\alpha\alpha}(\omega,\theta,E,\alpha)}{\sum_n \int_{\omega_{LC}}^{\omega_{UC}} \mathrm{d}\omega \int_0^{\pi} \mathrm{d}\theta D^n_{\alpha\alpha}(\omega,\theta,E,\alpha)}, \tag{4}$$

where E and α are the electron kinetic energy and pitch–angle, and $D^n_{\alpha\alpha}(\omega,\theta,E,\alpha)$ is the partial pitch–angle diffusion coefficient. Note that the resonances $\pm n$ come together because the ω–term can be omitted in the quasilinear resonance condition, $\omega - k_{\|}v_{\|} - n\Omega_e/\gamma = 0$, [e. g., *Summers and Thorne,* 2003], and the wave spectra are symmetric around $\theta = 90°$. The "Gauss" lines in Figure 1 show the result of a Gaussian distribution over x, and reproduce the equatorial diffusion coefficients of *Albert* [2003, Figure 6].

For all energies, Case A is slightly less than "Gauss" if only $|n| = 1$ resonances operate but in the region of $|n| > 1$ it is about 5 times greater than "Gauss" (Figure 1(c) and 1(d)). These dependencies are in good agreement with the previous results of *Albert* [2003, Figure 10, the second row]. For both "Gauss" and Case A, as follows from the

second row in the Figure 1, the contribution from $n < 0$ is negligible compared to the contribution from $n > 0$, especially for lower electron energies (see Figure 1(a) and 1(b)). Cases B and C further increase the EMIC wave normal angle, which further suppress the resonances $|n| = 1$, and shrink the region of pitch–angles subject to diffusion for low energies (see Figure 1(a) and 1(b)). At the same time, they increase by orders of magnitude the contribution from $|n| > 1$ which operate for greater electron energies, and increase the pitch–angle region subject to diffusion (see Figure 1(c) and 1(d)). The growing contribution of resonances with $n < 0$ is more pronounced in Cases B and C because EMIC waves become more elliptically polarized with the increase in the wave normal angle. The above results are in good qualitative agreement with the results by *Glauert and Horne* [2005] obtained for the H^+–mode of EMIC waves.

Overall, compared to field–aligned waves, the intermediate and highly oblique wave distributions decrease the pitch–angle range subject to diffusion, and reduce the scattering rate by orders of magnitude for low energy electrons ($E < 2$ MeV) when only principle $|n| = 1$ resonances operate. For greater electron energies (see Figure 1(c) and 1(d)), the $|n| = 1$ resonances operate only in a narrow region at large pitch-angles, and despite their greatest contribution for the field–aligned waves, cannot support electron diffusion into the loss cone. In this case, the oblique waves with $|n| > 1$ resonances are more effective, and extend the range of pitch–angle diffusion down to the loss cone. So EMIC waves alone, if distributed over the entire wave normal angle region, are able to cause local precipitation of energetic electrons.

4. Bounce–Average Diffusion Coefficient: Self–Consistent Calculations

4.1. Wave Normal Angle Distributions for He^+–mode of EMIC Waves

To analyze the wave normal angle characteristics, in this Section we use the results from a self–consistent thoretical model of RC and EMIC waves by *Khazanov et al.* [2006a]. The model is governed by a set of quasilinear and ray tracing equations, which explicitly includes the wave generation and damping, propagation, refraction, and reflection/tunneling in a multi–ion magnetospheric plasma. From a simulation of the May 1998 storm, *Khazanov et al.* [2006a] found that the equatorial He^+–mode energy distributions are not Gaussian over the wave normal angles, and that the wave energy can occupy not only the source region, i. e. the region of small wave normal angles, but all wave normal angles, including those near 90°. This is caused by energy outflow from the region of small wave normal angles to $\theta_0 = \pi/2$, which is due to the wave bouncing between surfaces of the bi–ion hybrid frequency in opposite hemispheres. Because the EMIC wave growth rate maximizes for the wave normal angle $\theta_0 = 0$, and because electron Landau damping has a peak for θ_0 close to 90°, the resulting wave normal angle distribution depends on ratios between the rates of wave growth (mostly in the region of small θ_0), Landau damping (mostly at large θ_0), and energy outflow rate, $\dot{\theta}_0/\theta_0$. Figure 2 shows the energy distribution over the equatorial wave normal angle for the He^+–mode EMIC waves. All the magnetic field spectra shown are in the postnoon–dusk MLT sector, 48 hours after 0000 UT on 1 May, 1998. Case (a) demonstrates a typical

Figure 2

quasi field–aligned wave normal angle distribution, where wave growth rate in the region of small θ_0 dominates the outflow toward greater θ_0. The diametrically opposite case is given by line (c), where EMIC wave energy is concentrated in the region of large θ_0. An intermediate case (b) corresponds to a situation when all the time scales have the same order of magnitude. Although power spectral density in that case drops for $\theta_0 > 40°$, there is still a very large $B^2(\nu, \theta_0)$, and we observe a broad distribution in the entire wave normal angle region.

Figure 2 shows spectra at one time and at three spatial points only, but would be interesting to see the wave power spectral density distributions on global spatial and temporal scales. In order to provide such a global view during the May 1998 storm, we calculate the average equatorial wave normal angle,

$$\left\langle \theta_0 \left(r_0, \varphi, t\right) \right\rangle = \frac{\int_{\omega_{min}}^{\omega_{max}} \mathrm{d}\omega \int_0^{\pi} \mathrm{d}\theta_0 B^2 \left(r_0, \varphi, t, \omega, \theta_0\right) \theta_0}{\int_{\omega_{min}}^{\omega_{max}} \mathrm{d}\omega \int_0^{\pi} \mathrm{d}\theta_0 B^2 \left(r_0, \varphi, t, \omega, \theta_0\right)}, \tag{5}$$

using the results from *Khazanov et al.* [2006a, Figure 6], where r_0, φ, t, ω, θ_0, and B are the radial distance in the magnetic equatorial plane, MLT, time, wave frequency, equatorial wave normal angle, and the wave magnetic field. Results are presented in Figure 3. The highly oblique waves with $\langle\theta_0\rangle > 50°$ are mainly observed in the noon–dusk MLT sector for high L–shells (in the plasmaspheric drainage plume), and an extremely oblique wave propagation with $\langle\theta_0\rangle > 80°$ is found in hour 33 (L=6.25, MLT=14) and 34 (L=5.75, MLT=13) snapshots. Although events with $\langle\theta_0\rangle < 50°$ are not well separated spatially from oblique waves, there is a tendency for them to be localized preferentially along the more narrow nightside plasmapause (compare Figure 3

Figure 3

with the density distribution in Figure 7 of *Khazanov et al.* [2006a]), especially for field–aligned events with $\langle\theta_0\rangle < 30^\circ$ (see the first row in Figure 3). The occurrences of the oblique and field–aligned wave normal angle distributions appear to be nearly equal during the May 1998 storm with slight dominance of oblique events.

The theoretical results clearly demonstrate that stormtime EMIC wave normal angle distributions are highly variable both in space and time, and that equatorial distributions range from field–aligned distributions through highly oblique distributions, which are in qualitative agreement with the results of *Anderson et al.* [1996] and *Denton et al.* [1996].

4.2. Diffusion Coefficient

To compare with Section 3, we now calculate the bounce–average pitch–angle diffusion coefficients using the plasma and wave parameters from the self–consistent model of *Khazanov et al.* [2006a, 2006b]. In order to calculate the diffusion coefficients, we use the simulation results at 48 hours after 0000 UT on 1 May, 1998 only. The He^+–mode EMIC wave spectra are shown in Figure 2 ($B^2_{(a)} = 28.6$ nT^2, $B^2_{(b)} = 41.6$ nT^2, and $B^2_{(c)} = 16.3$ nT^2) for this moment. The ion composition employed by *Khazanov et al.* [2006a], is 77% H^+, 20% He^+, and 3% O^+, and so will be used below for the diffusion coefficient calculation. For selected points, the equatorial values of $(\omega_{pe}/\Omega_e)^2$ are in the range 105–160. So we expect the electron minimum resonant energy to be greater than in Figure 1 (which depends on $(\omega_{pe}/\Omega_e)^2$, and for the He^+–mode on concentration of He^+ [*Summers and Thorne,* 2003]). The results are shown in Figure 4. Figure 4

While not as impressive as Figure 1, it has the advantage of being self–consistent. First of all, we see that the oblique lowest frequency wave distribution in Figure 2(c) cannot scatter electrons with energies below 10 MeV (actually, there are the regions of small Landau scattering for all energies with $\langle D_{\alpha\alpha} \rangle < 10^{-4}$ sec^{-1}), and spectra in Figures 2(a) and 2(b) scatter only the electrons with energies near 5 MeV and above. Second, the red lines in Figure 4 lie higher than the green lines, which is caused by the spectrum in Figure 2(b) having less energy in the field–aligned normal angles than the spectrum in Figure 2(a). This result for bounce–average coefficients is qualitatively consistent with the results in Figures 1(a) and 1(b) for the equatorial diffusion coefficients.

5. Summary and Conclusions

Precipitation due to resonant pitch–angle scattering by EMIC waves is one of the most important loss mechanisms of the outer RB electrons. Although suggested about three and half decades ago, only recently have balloon–borne X–ray observations provided strong evidence on the ability of EMIC waves to scatter outer RB relativistic electrons. These observations stimulated theoretical and statistical studies which demonstrated that this mechanism can operate in the strong diffusion limit for MeV electrons, and can compete with the adiabatic *Dst* effect during the initial and main phases of a storm.

Although the effectiveness of relativistic electron scattering by EMIC waves depends strongly on the wave spectral properties, unrealistic assumptions regarding the wave angular distribution were made in most previous theoretical studies. Namely, strictly

field–aligned or quasi field–aligned EMIC waves were only considered. The growing experimental and theoretical evidence that EMIC waves can be highly oblique has compelled us to study the effect of the wave normal angle characteristics on the outer RB relativistic electron scattering. In this study, we have calculated the equatorial and bounce–average pitch–angle diffusion coefficients for those electrons using for the H^+–mode of EMIC waves both the model (prescribed) and self–consistent distributions over the wave normal angle. Our results can be summarized:

1. In contrast to field–aligned waves, the intermediate and highly oblique wave distributions reduce the pitch–angle range subject to diffusion, and strongly decrease the scattering rate for low energy electrons ($E < 2$ MeV) when only principle resonances $|n| = 1$ operate (see Figures 1(a) and 1(b)).

2. For electron energies greater than ~ 5 MeV, the resonances $|n| = 1$ operate only in a narrow region at large pitch-angles (see Figure 1(c) and 1(d)), and despite their greatest contributions for field–aligned waves, cannot support electron diffusion into the loss cone. For those energies, oblique waves operating the $|n| > 1$ resonances are more effective, extending the range of pitch–angle diffusion down to the loss cone, and increasing the diffusion at lower pitch–angles by orders of magnitude.

Acknowledgments. This research was performed while K. Gamayunov held a NASA Postdoctoral Program appointment at NASA/MSFC. Funding in support of this study was provided by NASA grant UPN 370–16–10 and NASA HQ POLAR Project.

References

Albert, J. M. (2003), Evaluation of quasi–linear diffusion coefficients for EMIC waves in a multispecies plasma, *J. Geophys. Res., 108,* A6, 1249, doi:10.1029/2002JA009792.

Anderson, B. J., R. E. Denton, and S. A. Fuselier (1996), On determining polarization characteristics of ion cyclotron wave magnetic field fluctuations, *J. Geophys. Res., 101,* 13195.

Anderson, B. J., R. E. Erlandson, and L. J. Zanetti (1992), A statistical study of Pc 1–2 magnetic pulsations in the equatorial magnetosphere: 2. Wave properties, *J. Geophys. Res., 97,* 3089.

Arthur, C. W., R. L., McPherron, and J. D. Means (1976), A comparative study of three techniques for using spectral matrix in wave analysis, *Radio Sci., 11,* 833.

Denton, R. E., B. J. Anderson, G. Ho, and D. C. Hamilton (1996), Effects of wave superposition on the polarization of electromagnetic ion cyclotron waves, *J. Geophys. Res., 101,* 24869.

Foat, J. E., R. P. Lin, D. M. Smith, F. Fenrich, R. Millan, I. Roth, K. R. Lorentzen, M. P. McCarthy, G. K. Parks, and J. P. Treilhou (1998), First detection of a terrestrial MeV X–ray burst, *Geophys. Res. Lett., 25,* 4109.

Fraser, B. J. (1985), Observations of ion cyclotron waves near synchronous orbit and on the ground, *Space Sci. Rev., 42,* 357.

Fraser, B. J., and T. S. Nguyen (2001), Is the plasmapause a preferred source region of electromagnetic ion cyclotron waves in the magnetosphere?, *J. Atmos. Sol. Terr.*

Phys., 63, 1225.

Glauert, S. A., and R. B. Horne (2005), Calculation of pitch angle and energy diffusion coefficients with the PADIE code, *J. Geophys. Res., 110,* A04206, doi:10.1029/2004JA010851.

Green, J. C., T. G. Onsager, T. P. O'Brien, and D. N. Baker (2004), Testing loss mechanisms capable of rapidly depleting relativistic electron flux in the Earth's outer radiation belt, *J. Geophys. Res., 109,* A12211, doi:10.1029/2004JA010579.

Hoppe, M. M., C. T. Russell, T. E. Eastman, and L. A. Frank (1982), Characteristics of the ULF waves associated with upstream ion beams, *J. Geophys. Res., 87,* 643.

Ishida, J., S. Kokubun, and R. L. McPherron (1987), Substorm effects on spectral structures of Pc 1 waves at synchronous orbit, *J. Geophys. Res., 92,* 143.

Kim, H.–J., and A. A. Chan, Fully adiabatic changes in storm time relativistic electron fluxes (1997), *J. Geophys. Res., 102,* 22107.

Khazanov, G. V., K. V. Gamayunov, D. L. Gallagher, and J. U. Kozyra (2006a), Self–consistent model of magnetospheric ring current and propagating electromagnetic ion cyclotron waves: Waves in multi ion magnetosphere, *J. Geophys. Res., 111,* A10202, doi:10.1029/2006JA011833.

Khazanov, G. V., K. V. Gamayunov, D. L. Gallagher, M. W. Liemohn, and J. U. Kozyra (2006b), Self–consistent model of magnetospheric ring current and propagating electromagnetic ion cyclotron waves. 2. Wave induced ring current precipitation and thermal electron heating, *J. Geophys. Res.,* in press.

Khazanov, G. V., K. V. Gamayunov, and V. K. Jordanova, Self–consistent model

of magnetospheric ring current ions and electromagnetic ion cyclotron waves: The 2–7 May 1998 storm (2003), *J. Geophys. Res., 108*, A12, 1419, doi:10.1029/2003JA009856.

Li, X., D. N. Baker, M. Temerin, T. E. Cayton, G. D. Reeves, R. A. Christiansen, J. B. Blake, M. D. Looper, R. Nakamura, and S. G. Kanekal (1997), Multi–satellite observations of the outer zone electron variation during the November 3–4, 1993, magnetic storm, *J. Geophys. Res., 102,* 14123.

Lorentzen, K. R., M. P. McCarthy, G. K. Parks, J. E. Foat, R. M. Millan, D. M. Smith, R. P. Lin, and J. P. Treilhou (2000), Precipitation of relativistic electrons by interaction with electromagnetic ion cyclotron waves, *J. Geophys. Res., 105,* 5381.

Loto'aniu, T. M., R. M. Thorne, B. J. Fraser, and D. Summers (2006), Estimating relativistic electron pitch angle scattering rate using properties of the electromagnetic ion cyclotron wave spectrum, *J. Geophys. Res., 111,* A04220, doi:10.1029/2005JA011452.

Lyons, L. R., and R. M. Thorne (1972), Parasitic pitch angle diffusion of radiation belt particles by ion cyclotron waves, *J. Geophys. Res., 77,* 5608.

Means, J. D. (1972), Use of three–dimensional covariance matrix in analyzing the polarization properties of plane waves, *J. Geophys. Res., 77,* 5551.

Meredith, N. P., R. M. Thorne, R. B. Horne, D. Summers, B. J. Fraser, and R. R. Anderson (2003), Statistical analysis of relativistic electron energies for cyclotron resonance with EMIC waves observed on CRRES, *J. Geophys. Res., 108,* A6,

1250, doi:10.1029/2002JA009700.

Millan, R. M., R. P. Lin, D. M. Smith, K. R. Lorentzen, and M. P. McCarthy (2002), X–ray observations of MeV electron precipitation with a balloon–borne germanium spectrometer, *Geophys. Res. Lett., 29*(24), 2194, doi:10.1029/2002GL015922.

Reeves, G. D., K. L. McAdams, R. H. W. Friedel, and T. P. O'Brien (2003), Acceleration and loss of relativistic electrons during geomagnetic storms, *Geophys. Res. Lett., 30*(10), 1529, doi:10.1029/2002GL016513.

Schwarz, S., and R. E. Denton (1991), XWHAMP–Waves in homogeneous, anisotropic, multicomponent plasmas, Northstar software documentation, Nortstar, Dartmouth Coll., Hanover, NH.

Summers, D., C. Ma, and T. Mukai (2004), Competition between acceleration and loss mechanisms of relativistic electrons during geomagnetic storms, *J. Geophys. Res., 109,* A04221, doi:10.1029/2004JA010437.

Summers, D., and R. M. Thorne (2003), Relativistic electron pitch–angle scattering by electromagnetic ion cyclotron waves during geomagnetic storms, *J. Geophys. Res., 108,* A4, doi:10.1029/2002JA009489.

Thorne, R. M., and R. B. Horne (1992), The contribution of ion–cyclotron waves to electron heating and SAR–arcs excitation near the storm–time plasmapause, *Geophys. Res. Lett., 19,* 417.

Thorne, R. M., R. B. Horne, S. A. Glauert, N. P. Meredith, Y. Y. Shprits, D. Summers, and R. R. Anderson (2005), The influence of wave–particle interactions on relativistic electron dynamics during storms, in *Inner Magnetosphere*

Interactions: New Perspectives From Imaging, Geophys. Monogr. Ser., vol. 159, edited by J. Burch, M. Schulz, and M. Spence, pp. 101–112, AGU, Washington, D. C.

Thorne, R. M., and C. F. Kennel (1971), Relativistic electron precipitation during magnetic storm main phase, *J. Geophys. Res., 76,* 4446.

Young D. T., S. Perraut, A. Roux, C. de Villedary, R. Gendrin, A. Korth, G. Kremser, and D. Jones (1981), Wave–particle interactions near Ω_{He^+} observed on GEOS 1 and 2: 1. Propagations of ion cyclotron waves in He^+–rich plasma, *J. Geophys. Res., 86,* 6755.

K. V. Gamayunov, National Space Science and Technology Center, NASA Marshall Space Flight Center, Space Science Department, 320 Sparkman Drive, Huntsville, AL 35805, USA. (e–mail: konstantin.gamayunov@msfc.nasa.gov)

G. V. Khazanov, National Space Science and Technology Center, NASA Marshall Space Flight Center, Space Science Department, 320 Sparkman Drive, Huntsville, AL 35805, USA. (e–mail: george.khazanov@msfc.nasa.gov)

Received _____

Figure 1. Equatorial diffusion coefficients versus equatorial pitch–angle for scattering of relativistic electrons by the He^+–mode of EMIC waves. The wave spectrum parameters and ion content are given in the text, L=4, and $(\omega_{pe}/\Omega_e)^2 = 10^3$, where ω_{pe} and Ω_e are the electron plasma frequency and gyrofrequency (without Lorentz factor), respectively. The curve "Gauss" is obtained for a wave normal angle distribution adopted by *Albert* [2003]. The second row shows the corresponding average resonant numbers (see the text for definition).

Figure 2. Equatorial power spectral densities for the He^+–mode EMIC waves from simulation by *Khazanov et al.* [2006a]. All the squared magnetic field spectra are obtained at 48 hours after 0000 UT on 1 May, 1998. (a) L=5.25, MLT=16, (b) L=5.75, MLT=15, and (c) L=5.75, MLT=14.

Figure 3. Average equatorial wave normal angle for the He^+–mode EMIC waves during the May 1998 event. The specified hours are counted from 0000 UT on 1 May, 1998.

Figure 4. The bounce–average diffusion coefficients for relativistic electron scattering by the He^+–mode of EMIC waves. The wave spectra are taken from simulation by *Khazanov et al.* [2006a], and shown in Figure 2. The ion percentage is 77% of H^+, 20% of He^+, and 3% of O^+, and the equatorial values for factor $(\omega_{pe}/\Omega_e)^2$ are 105, 160, and 138 for the red, green, and blue lines, respectively.

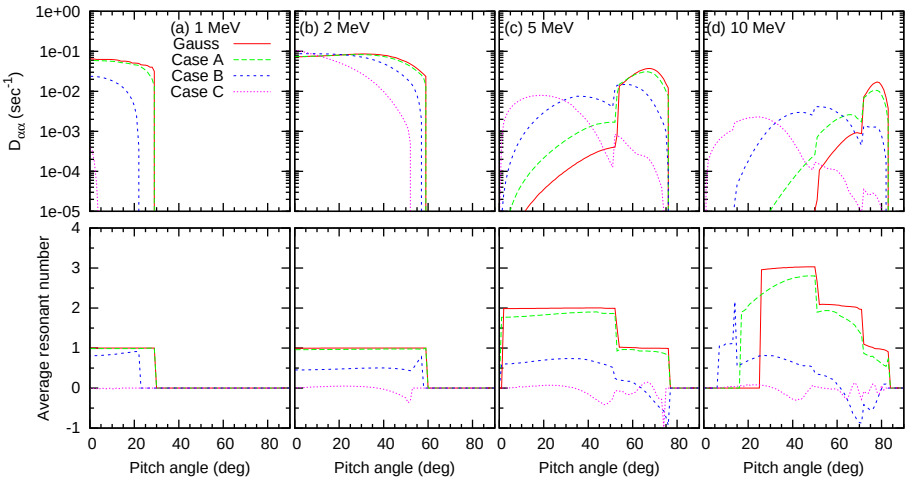
(a) 1 MeV
(b) 2 MeV
(c) 5 MeV
(d) 10 MeV
Gauss
Case A
Case B
Case C
$D_{\alpha\alpha}$ (sec^{-1})
Average resonant number
Pitch angle (deg)

Figure 1.

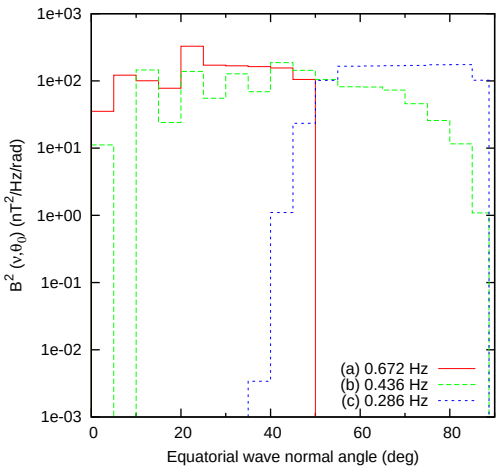
1e+03
1e+02
1e+01
1e+00
1e-01
1e-02
1e-03
0
20
40
60
80
B2 (v,θ0) (nT2/Hz/rad)
Equatorial wave normal angle (deg)
(a) 0.672 Hz
(b) 0.436 Hz
(c) 0.286 Hz

Figure 2.

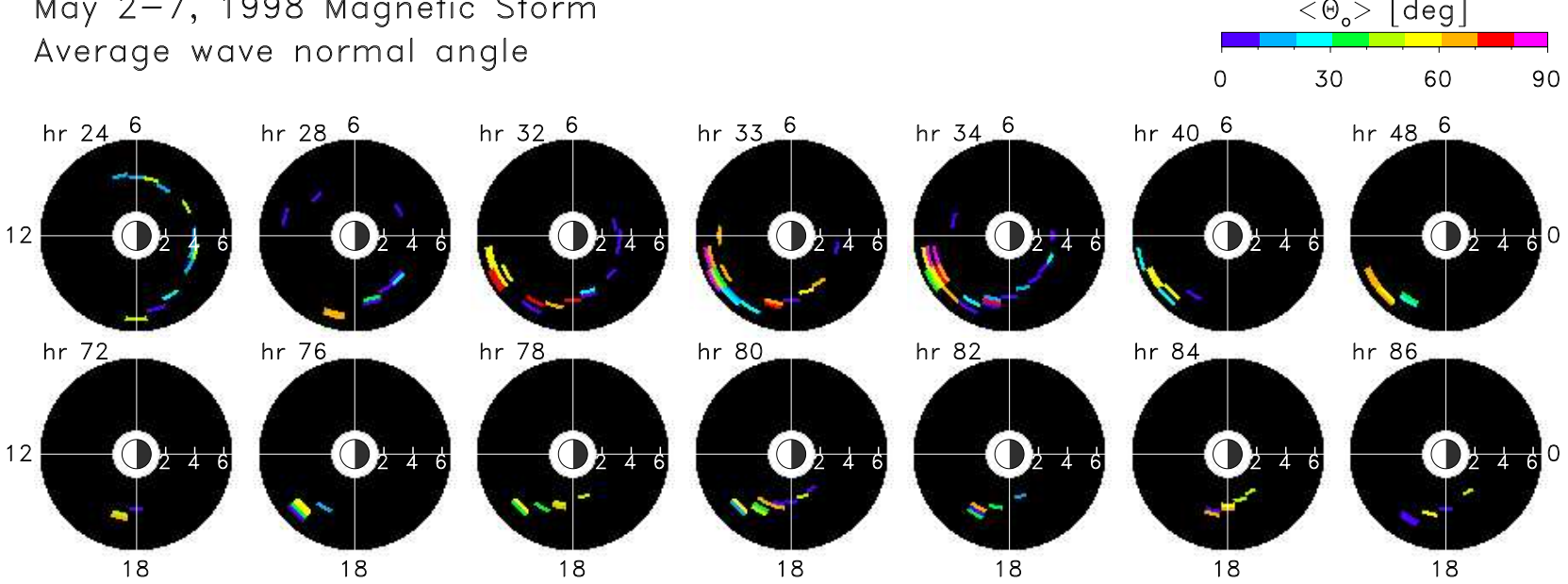
May 2–7, 1998 Magnetic Storm
Average wave normal angle
<Θo> [deg]
0
30
60
90
hr 24
hr 28
hr 32
hr 33
hr 34
hr 40
hr 48
hr 72
hr 76
hr 78
hr 80
hr 82
hr 84
hr 86
6
12
0
18
2
4
6

Figure 3.

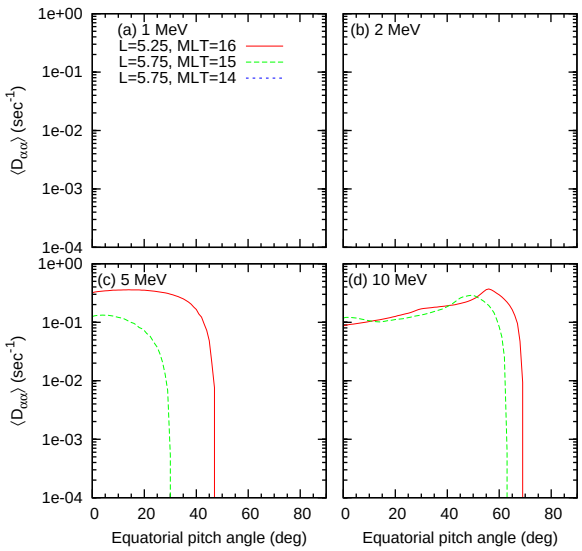
(a) 1 MeV
L=5.25, MLT=16
L=5.75, MLT=15
L=5.75, MLT=14
(b) 2 MeV
(c) 5 MeV
(d) 10 MeV
⟨Dαα⟩ (sec-1)
1e+00
1e-01
1e-02
1e-03
1e-04
0
20
40
60
80
Equatorial pitch angle (deg)

Figure 4.